An Deng and Yang Xiao

Measuring and modeling proportion-dependent stress-strain behavior of EPS-sand mixture

International Journal of Geomechanics, 2010; 10(6):214-222

http://dx.doi.org/10.1061/(ASCE)GM.1943-5622.0000062

Measuring and Modeling Proportion Dependent Stress-Strain Behavior of EPS-Sand Mixtures

An Deng[1,2 *] and Yang Xiao[1,2]

[1] Key Laboratory of MOE for Geomechanics and Embankment Engineering, Hohai University, Nanjing 210098, China;

[2] Geotechnical Research Institute, Hohai University, Nanjing 210098, China;

* Corresponding author: a_deng@hhu.edu.cn

ABSTRACT: A geofoam was produced by blending expanded polystyrene (EPS) beads and sands in proportions. The formed mixtures, known as EPS-sands, were 32-66% lighter than general earthfills (e.g., sand). Consolidated-drained (CD) triaxial compression tests were conducted on EPS-sand mixture specimens to observe their stress-strain characteristics, specifically, the stress-strain responses in relation to the EPS contents (0.5%, 1.5% and 2.5% by weight) used in the mixtures and confining pressures (100, 200, 300 to 400 kPa) loaded on the specimens. The EPS content and confining pressure were found to influence the stress-strain and volumetric strain behavior of the mixtures. Increasing EPS content led to decreased shear strength and increased volumetric strain. Increasing confining pressures enhanced the strength of the mixture. EPS-sand mixtures underwent a shear contraction throughout the CD tests. The optimum EPS bead content (i.e., the one reasonably balancing the unit weight, strength and deformation) was in the order of 0.5% by weight. EPS content dependent strain

increment equations were derived by compromising Cam-clay and Modified Cam-clay, and used to model the stress-strain characteristics of EPS-sand mixtures. The established equations were verified being able to depict the stress-strain observations of EPS-sand specimens, at least for the ranges of EPS contents and confinements considered in this study.

Keywords: EPS beads; sands; triaxial compression; shear strength; Cam-clay; stress-strain behavior; lightweight fills.

INTRODUCTION

Geofoam has been acknowledged, relative to its low unit weight, as an attractive choice of substitute for earthfills in special infrastructure works, e.g., widened embankments, abutments or bridge approaches, retaining works and flexible pipeline backfills (Horvath 1994; Duskov 1997; Greeley 1997). The replacements with geofoam were able to mitigate the vertical stresses imposed onto underlying (difficult) soils (Horvath 1994, 1997, 2008; Doskov 1997; Snow and Nickerson 2004) or flexible utilities pipelines, as well as to reduce the lateral stresses loaded onto the side-way earth structures (Hazarika and Okuzono 2004; Horvath 2004). In practice, geofoam also demonstrated favorable performances in buffering mechanical impacts, e.g., swelling of expansive soil (Aytekin 1997; Ikizler et al. 2008) and seismic vibrations (Riad and Horvath 2004; Zarnani et al. 2009), as well as in mitigating thermal distresses in permafrost regions (Wen et al. 2008).

Geofoam can be either prefabricated expanded polystyrene (EPS) block (Horvath 1994, 1997, 2008; Doskov 1997), or the mixture of soils and EPS pre-puff beads (Liu et al. 2006; Zhu et al. 2008). Both need to be investigated with respect to measuring and modeling their stress-strain characteristics so as to evaluate the field design and construction. To date, investigations regarding EPS blocks can be reached through many sources, for examples, field and laboratory measurements (Doskov 1997; Fang et al. 2006), and modeling analyses (Chun et al. 2004; Hazarika and Okuzono 2004; Wang et al. 2006; Wong and Leo 2006; Hazarika 2006). There were also reports in the public domain about the measurements of soil-EPS-cement mixtures (Liu et al. 2006; Zhu et al. 2008)), whereas no implementation was reported on measuring and modeling the stress-strain behavior of soil-EPS beads mixtures.

In this study, EPS beads and construction sands were blended homogeneously in proportions to form nonstructural granular lightweight fills, referred to as EPS-sand hereafter. The non-cementitious lightweight fills not only save the use of cement, but also were suitable for works where low strength and instant excavation were desired. The goal of this study was to measure the stress-strain characteristics of EPS-sand mixtures, as well as to model the proportion dependent stress-strain behavior of the mixtures. Laboratory consolidated-drained (CD) triaxial compression tests were conducted on EPS-sand specimens prepared at designated EPS contents and subjected to varying confining pressures. The stress-strain responses of the mixtures were observed, collected and analyzed. Proportion dependent strain increment equations were derived and verified to depict the strength and deformation behavior of EPS-sand.

MATERIALS AND METHODS

Sand and EPS Bead

The sand used in the EPS-sand matrix was general construction fine sand and supplied by a professional construction material company in Nanjing China. The index properties of the sand are presented in Table 1. The water content as-received of sand was 5%. The particle size distribution for the sand is shown in Fig. 1. The sand had a coefficient of uniformity of 6.7, a coefficient of curvature of 1.3, and was classified under the Unified Soil Classification System as SW (well graded sand) and under the AASHTO (American Association of State Highway and Transportation Officials) Soil Classification System as A-3 (0). It had a specific gravity of 2.62, a maximum dry unit weight of 18.9 kN/m^3 (i.e., minimum void ratio of 0.39) and a minimum dry unit weight of 15.4 kN/m^3 (i.e., maximum void ratio of 0.70). The friction angle of the sand was 32.6° when its relative density D_r was 50%.

EPS bead is a super light polymer foam, pre-puffed from polystyrene resin. The EPS beads used in this study were provided from a professional supplier which had been manufacturing EPS geofoam blocks. The beads were white, even and spherical, sizing between 2-4 mm (Fig. 2).

Determinations of the unit weight and specific gravity of the EPS beads were conducted by a means modified from comparable standard test method for fine aggregates (i.e.,

ASTM C128). Beads were placed into a 1-L hydrometer until the volume of the hydrometer was apparently occupied. The placement was implemented without much compaction but light tilting effort, which basically simulated the moderate compaction the beads should reach. Scale and calculate the net weight of beads used to fill the hydrometer, and determine the unit weight through dividing the net weight by the volume (1 L). The unit weight obtained for EPS beads was 0.15 kN/m^3. Next, cover the opening of the hydrometer with a piece of gauze, and hoop the gauze around the hydrometer with an O-ring. Add de-aired water volume into the hydrometer through the gauze until the hydrometer weight was constant. Calculate the absolute volume occupied by the beads in the hydrometer and determine the specific gravity of beads, which was 0.03.

EPS-Sand Specimen Preparation

EPS-sand specimens (Fig. 2) were formed by mixing EPS beads with sands at a dry mass ratio η of EPS beads over sands, which was thought as the most significant factor controlling the unit weight and mechanical behavior of the mixtures. Investigated ratios were 0.5%, 1.5% and 2.5%. Water content of 10% was controlled in each mixture to facilitate the compaction in the next step. For each designated mixing ratio, the mass-based proportions of sand, EPS bead and water were determined aforehand. The proportioned materials were mixed thoroughly using an air-mixing method. That is, mixtures were placed into an air-tight plastic bag and subjected to manual vibration efforts until the mixtures were homogeneous enough, normally, taking 3-5 minutes dependent on the mixture volume.

Triaxial cylindrical specimens were prepared at a diameter of 39.1 mm (1.5 in.) and a height of 80 mm (3.1 in.). The sample size ratio is defined as the diameter of the specimen divided by the maximum particle size. As the sample size ratio approached 20 for sand and 10 for EPS bead, respectively, the effects of sample size became negligible (Marachi et al. 1972; Indraratna et al. 1993). Mixtures at a designated weight were placed into a split mold and compacted moderately by vibrating and tamping efforts until the desired relative density (i.e., D_r=50%) was reached. Specifically, the target relative density of EPS-sand matrix was achieved by quantifying the weight of proportioned EPS and sand mixtures to be placed within a volume (i.e., 39.1×80 mm). Compaction was completed in three increments (i.e., 30, 30 and 20 mm in sequences). Consistent compaction was attained by controlling the feed quantity of the portion to be placed in an increment. The specimen preparation procedure used in this study was implemented to obtain a homogeneous distribution, and no evidence of segregation was observed for any EPS content. Consequently, interpretation of the test results assumed homogeneity of the specimens.

Triaxial Apparatus

A standard strain-controlled triaxial apparatus was used in this investigation to test specimens. A schematic diagram of the triaxial cell is shown in Fig. 3. The cell consisted of three principal components, namely: the base, the chamber, and the top head of the cell. The base, i.e., the pedestal, where the specimen rested, incorporated three separate

inlet/outlet connections. One connection was used to supply de-aired water into the chamber and to pressurize the water to obtain the desired cell pressure. The other two connections were linked exclusively to the specimen. The bottom one was used in combination with a pressure transducer to measure the pore-water pressure in the undrained tests, and the top one was used to flush water to remove air bubbles during specimen preparation and drain water in shear in the drained tests. Indeed, the bottom line was sometimes used to apply a back pressure to saturate the specimen during specimen preparation. At the top part of the cell, a displacement transducer and a load ring were installed to obtain the deformation and force acting on the specimens.

Aside from the triaxial cell, there were peripheral devices attached to the triaxial cell for the triaxial apparatus to implement the tests. For examples, a gear box was used to control the axial strain rate. A pressure meter was used to measure and maintain cell pressures applied during tests. Changes in water level in an attached burette were collected and inspected to correlate to volume changes in the specimens. The axial load was correlated to the system vertical compressions and ring deformations which were monitored through the gauges installed on the triaxial system. The details of a triaxial apparatus can be referred to the laboratory manual by Bowles (1992).

TESTING PROGRAM

The testing program is summarized in Table 2. A total of 4 series (i.e., EPS content η=0 (pure sand), 0.5%, 1.5% and 2.5%, respectively) of CD triaxial compression tests were

performed as part of this investigation. Series 1 was conducted using pure sand specimens. Series 2 to 4 were conducted using EPS-sand specimens. Each series included 4 cylindrical specimens, which, before shear, were subjected to 4 separate consolidation pressures, respectively (i.e., 100 kPa, 200 kPa, 300 kPa and 400 kPa). The unit weight of the EPS-sand mixture was found to be less than that of moderately compacted sand by about 12-32% per 0.5% EPS inclusion depending on the mixing ratio. The volumetric ratio of EPS over the combination of EPS and sand in the mixture, ς, was calculated based on the mixing ratios and specific gravities of particles for each mixture, as presented in Eq. 1. EPS-sand mixture prepared at EPS content η=0.5% by weight had approximately 30% EPS in volume. If the EPS content increased to 1.5% or above, the EPS volumetric ratio exceeded 57%, which substantially led to reduced sand-sand interactions.

$$\varsigma = \frac{\dfrac{\eta}{G_{\mathrm{sEPS}}}}{\dfrac{100}{G_{\mathrm{ss}}} + \dfrac{\eta}{G_{\mathrm{sEPS}}}} \tag{1}$$

where, ς denoting the EPS volumetric percentage in the mixture, G_{sEPS} and G_{ss} denoting the specific gravities of EPS bead and sand, respectively.

After placing the EPS-sand specimen (still encased in the steel mold) onto the pedestal of the triaxial cell, special procedures were implemented prior to taking off the mold. In deed, as the EPS-sand mixture was remolded and cohesionless, the specimen contained in the rubber membrane tended to collapse or deform by simply removing the mold. To

pre-stabilize the EPS-sand specimen, a negative pressure (suction) was supplied within the specimen by following procedures: 1) flush the specimen by allowing de-aired water to flow from the bottom of the specimen upwards to expel the majority of air bubbles out through the top drainage line; 2) close the valve of the top drainage line, open the valve of the bottom drainage line, which was connected to the barrette, and lower the water level in the barrette. The hydraulic gradient resulted in a negative pore water pressure generated in the specimen, when the mold can be taken off without excessively disturbing the stability of specimens.

Hydraulic gradient saturation was implemented on each specimen prior to consolidation. After assembling the triaxial cell, it was filled with de-aired water. A small quantity of vaseline was dabbed on top of the cell and around the piston to reduce the piston friction and to seal the chamber. Pressurize the cell de-aired water constant at 20 kPa. The specimen was flushed again upward to expel any air bubble remained in the specimen by generating an around 1-m hydraulic head difference across the specimen. The saturation was thought completed when air bubble did not escape from the top drainage line any more.

An isotropic consolidation stress was then applied to the specimen by increasing the cell pressure to the designated level. A time span of at least 2 h was allowed for any creep deformation to be completed. At the end of consolidation, the axial load was increased at a constant rate of axial strain of 0.015 mm/min or 0.019% strain/min, over which the pore

water pressure was controlled below 5 percent of consolidation pressure. The choice of the strain rate was made on the basis of 95% minimum pore-water pressure dissipation during loading (Head 1982). The tests were halted after the axial strain reached 15%, due to the difficulty of measuring large stains in the triaxial test. Beyond a 15% or higher strain, shape distortions of specimens were rather large due to excessive deformation and strain measurements became meaningless.

The failure defined to determine the stress conditions was taken to correspond to the maximum deviatoric stress attained or the deviatoric stress at 15% axial strain, whichever was obtained first during a test. It should be noted that the shear strength defined for specimens that did not show a well-defined peak deviatoric stress was sensitive to the strain level used to define failure.

As CD conditions were applied in triaxial compression tests, total stress responses and parameters were used throughout this study. Observations, as part of this investigation, included axial stress σ_a, axial strain ε_a and volumetric strain ε_v, which led to the relations of the deviatoric stress-axial strain, volumetric strain, and shear behavior of EPS-sand specimens. A detailed discussion regarding the effects on stress-strain characteristics of variables such as EPS content and confining pressures was provided in the following section. Special focus was placed on the evaluation of K_f lines and strength parameter. For each test series, two sets of shear strength parameters were estimated: a)

K_f line strength parameters; and b) conventional Mohr–Coulomb shear strength parameters.

Further focus was placed on the derivation of strain increment equations that were used to model the stress-strain responses and to govern strength and deformation calculations of infrastructure works in practice. Model verifications were given based on the CD triaxial compression test results.

RESULTS AND DISCUSSION

Deviatoric stress-axial strain-volumetric strain behavior

The deviatoric stress-strain and volumetric strain behavior of pure sand and EPS-sand specimens are presented in Figs. 4-7. Fig. 4 presents the stress-strain and volumetric strain behavior of pure sand specimens. The Figs. 5-6 present the stress-strain and volumetric strain behavior of EPS-sand specimens prepared with EPS contents of 0.5% and 1.5%, respectively. Fig. 7 presents the stress-strain behavior of EPS-sand specimens prepared with EPS contents of 2.5%, volumetric strain of which is not presented as the specimens experienced significant volumetric contraction during consolidation process and the volumetric strain data collected are not representative of real volumetric variation.

The deviatoric stress-strain and volumetric strain behavior observed on pure sand specimens show a dilatation behavior (Fig. 4). That is, pure sand at relative density of D_r=50% behaves as medium to dense sand do. Reasonably well defined peak shear strengths are indicated. The stress-strain responses are dependent on confining pressures. As confining pressures increase, the stress-strain curves indicate an increase in the initial slope and an increase in the peak strength. A clear strength jump is indicated between confinements of 200 kPa and 300 kPa. Volumetric strains at confining pressures (from 100 kPa to 400 kPa) show a slight contraction followed by dilation until the end of the test, and as expected, the dilation tends to be weakened along with the increase of the confining pressure.

The deviatoric stress-strain and volumetric strain behavior observed on EPS-sand specimens shows approximately hyperbolic stress-strain relations, as well as a fully contractive behavior for the different confining pressures used in this investigation (Figs. 5-7). Such contractive behavior of EPS-sand mixtures is different from the dilatant behavior obtained on sand (Fig. 4) and on rubber-sand mixtures obtained in previous investigations (Zornberg et al. 2004). It seems to indicate that the shear behavior of EPS-sand specimen changes from being dense/medium sand-like to being loose sand-like along with the EPS content increase. The contractive volumetric strains increase steadily and are not likely to reach their maximum, at least for axial strain up to 15%. Also, no clear peak shear strength was obtained in the same axial strain range. Beyond the axial strain range, the volumetric compression seems to keep escalating. In this context, the

shear stress at 15% axial strain was used as the peak shear strength value. Also, increasing confinement enhanced the shear strength of EPS-sand specimen, as was the case for the tests on pure sand specimen.

The peak shear strength obtained on EPS-sand specimen is less than the peak shear strength obtained on pure sand specimens all other variables maintained constant. Furthermore, as expected, the higher the EPS content, the lower the peak shear strength of the EPS-sand, which implicates that there is an optimum EPS content η balancing the unit weight and the shear strength desired for the mixtures. Secondly, the axial strains (up to 15%) at defined peak shear strengths for EPS-sand specimens (Figs. 5-7) are considerably higher than the axial strains (5%-7%) at peak strengths for pure sand specimens, all other variables maintained constant. No post-peak shear strength loss is shown in the test results, as all curves are strain-hardening types. Lastly, the entire stress-strain responses of EPS-sand specimens (series 2-4) are very similar, except for the magnitude of strength impairment along with EPS content variation.

Investigation of volumetric responses indicates that volumetric variation was highly dependent on the confining pressure acted on the specimens, as well as the EPS content η used to prepare the specimens. For examples, the EPS-sand specimens prepared at EPS content η=0.5% completed substantial volumetric contraction during consolidation (σ_3=400 kPa) and experienced distorted low contraction during shearing, which led to the inconsistency of its volumetric behavior with the volumetric responses of the other

specimens. Also, EPS-sand specimens prepared at η=1.5% or 2.5% presented similar volumetric responses, even under lower confinements (e.g., σ_3=100 to 300 kPa). In this context, the EPS-sand mixtures prepared at over 0.5% EPS content were not suitable for deformation sensitive works subjected to high confinements (e.g., σ_3>100).

K_f Line and Strength Parameter

Define (s, t) stress coordinate, where $s=(\sigma_1+\sigma_3)/2$, $t=(\sigma_1-\sigma_3)/2$. K_f line is obtained by interpolation through the failure points (s_f, t_f), resulting in a straight line represented by Eq. 2, and yielding two K_f line strength parameters (α, a). Generally, K_f line intercepts the origin, leading to a=0.

$$t_f = a + s_f \tan\alpha \tag{2}$$

where, $s_f=(\sigma_{1f}+\sigma_{3f})/2$, $t_f=(\sigma_{1f}-\sigma_{3f})/2$, α and a representing the slope and ordinate intercept of K_f line, respectively.

Fig. 8 presents the K_f line approximation in s-t plane for pure sand and EPS-sand specimens (at EPS contents η=0.5%, 1.5% and 2.5%, respectively). K_f lines are approximated linearly (R^2=0.99) for pure sand and EPS-sand (η=0.5%), as shown in Fig. 8(a), whereas K_f lines are reasonably approximated piecewise for EPS-sand mixtures prepared at η=1.5% and 2.5%. K_f line strength parameters (a, α) are presented in Table 3.

When the EPS contents are 0% (pure sand) and 0.5%, or probably range between 0% and 0.5%, the K_f line is linearly approximated intercepting the origin for the specimens tested under the confining pressures considered in this investigation (Fig. 8(a)). The K_f line slopes α are 31.4° for the pure sand specimen and 21.3° for the EPS-sand specimen (at η=0.5%), respectively, which means that the inclusion of EPS beads tends to impair the peak shear strength of materials.

When the EPS content increases to a level over 0.5% (e.g., 1.5% and 2.5%), the K_f line deviates from straight line correlation, and is reasonably characterized by an intercepted piecewise (in two segments) linear approximation (Fig. 8(b)). Such piecewise linear trend is approaching the shear behavior of over-consolidated soils. On top of this, two sets of K_f line parameters (α and a) were estimated to account for the lower and upper segments, respectively (Table 3). Also, it is noted that cohesive intercepts, instead of intercepting the origin, were obtained for K_f lines of EPS-sand specimens (at, or probably ranging between, η=1.5% and 2.5%).

Using the geometric relation between a Mohr Coulomb envelope and a K_f line, the envelope shear strength parameters (c and ϕ_{cd}) were obtained and presented in Table 3. As expected, the peak shear strength of EPS-sand decreases with increasing EPS content, although the unit weight behaves the opposite. Thus, it is not advised to use the EPS-sand

as structural fills where high strength is required. Indeed, as afore-commented, there is an optimum EPS content at which the EPS-sand is reasonably prepared by balancing the unit weight and shear strength of the mixture. According to the investigation, EPS-sand specimen prepared at η=0.5% presented reasonably acceptable performance, i.e., low unit weight (12.6 kN/m^3) and competitive shear strength (ϕ_{cd}=23°).

Results in Table 3 suggest that the shear mechanism in EPS-sand matrix experienced transition along with the increase of the EPS content. There were three principal shear mechanisms in terms of granular interaction types, i.e. sand-sand, sand-EPS and EPS-EPS. In course of increasing EPS content, shear mechanism within the EPS-sand matrix was governed by gradually weakening sand-sand interaction and strengthening sand-EPS and EPS-EPS interactions. Sand-sand shear mechanism yielded higher shear strength than sand-EPS and EPS-EPS mechanisms did, which was related to the particle rigidity difference between sands and EPS beads, as well as the packing difference among sand-sand, sand-EPS and EPS-EPS compositions. As such, shear mechanisms of sand-EPS and EPS-EPS began to govern the shear strength of the mixtures prepared at high EPS content (e.g., η>0.5%), however, leading to lower overall shear strength values.

The cohesive intercepts observed for EPS-sands at relatively high EPS contents (i.e., η=1.5% and 2.5%) suggest the presence of apparent cohesion within the matrix. As commented, sands were much harder than EPS beads. Consequently, the shear efforts enforced the sands partially or even completely intruded into EPS beads. An apparent

cohesion was rendered within the matrix. That is, a binding force was yielded within the EPS-sand matrix, which may possibly relate to the cohesion values obtained for EPS-sand specimens (at η=1.5% and 2.5%) tested in this investigation. A second interpretation was related to the consolidation-hardening mechanism occurred to EPS-sand mixtures tested under high confining pressures. Indeed, EPS beads experienced substantial volumetric compression during high pressure consolidation, which densified the mixtures remarkable more than a low consolidation pressure did. Accordingly, a more compact and rigid structure led to an increased shear strength gain.

Overall, the test results obtained in this study indicate that infrastructure backfilling works under comparatively low confining pressures (e.g., utility trench backfills) can benefit from the inclusion of EPS bead. From the materials and test conditions considered in this investigation, the optimum EPS content is in the order of 0.5%, at which the EPS-sand mixtures yield a reasonable combination of unit weight and shear strength.

MODEL DERIVATION

Notations

In this section, the stress coordinates (p, q) were defined as follows:

$$p = \frac{(\sigma_1 + 2\sigma_3)}{3} \tag{3}$$

$$q = \sigma_1 - \sigma_3 \quad (4)$$

where, p denoting mean stress, q denoting deviator stress, σ_1 and σ_3 denoting the major and minor principal stresses, respectively.

Cam-clay and Modified Cam-clay

Many constitutive models were proposed with regards to depicting the stress-strain behavior of soils. These models are largely divided into two types: elastic models and elasto-plastic models. The latter is more robust than the former to represent the soil behavior, e.g., strain hardening or softening characteristics, shear dilation and stress paths. One of the classical elasto-plastic models is Cam-clay. Cam-clay incorporated the critical state theory plus a series of plasticity concepts. In this section, the concepts and strain equations of Cam-clay models were briefly presented, but not deduced. A deep and a comprehensive review of plasticity and the deduction of Cam-clay strain equations should refer to the other sources, e.g., Schofield and Wroth (1968), Desai and Siriwardane (1984), and Ortigao (1995).

A soil element starts to yield when its effective stress path touches a particular convex surface defined in the stress coordinate (e.g., (p, q)), known as the yield locus. The yield loci are presented in Fig. 9(a) for Cam-clay and Fig. 9(b) for Modified Cam-clay, respectively. Variable p_m represents the isotropic consolidation pressure (i.e., σ_3). K_{cr}

represents the critical state line. Within the loci, all strains are assumed to be purely elastic. As the effective stress path touches the loci, a soil element starts to yield, and plastic strains will be added to the elastic strains. This study focused on the sum of elastic and plastic strains.

In Cam-clay, the volumetric strain increment (in differentiation), $\mathrm{d}\varepsilon_{\mathrm{v}}$, shear strain increment, $\mathrm{d}\varepsilon_{\mathrm{s}}$, and axial strain increment, $\mathrm{d}\varepsilon_{\mathrm{a}}$, are defined in Eqs. 5-7, respectively.

$$\mathrm{d}\varepsilon_{\mathrm{v}} = \frac{1}{1+e}\left[\frac{\lambda-\kappa}{Mp}\left(\mathrm{d}q - \frac{q\mathrm{d}p}{p}\right) + \lambda\frac{\mathrm{d}p}{p}\right] \tag{5}$$

$$\mathrm{d}\varepsilon_{\mathrm{s}} = \frac{\lambda-\kappa}{(1+e)Mp}\left[\frac{\mathrm{d}q}{M-(q/p)} + \mathrm{d}p\right] \tag{6}$$

$$\mathrm{d}\varepsilon_{\mathrm{a}} = \mathrm{d}\varepsilon_{\mathrm{s}} + \frac{1}{3}\mathrm{d}\varepsilon_{\mathrm{v}} \tag{7}$$

where, e denoting initial void ratio, λ denoting the absolute slope of normal consolidation line in $v-\ln p$ coordinate, κ denoting the absolute slope of swelling (over-consolidation) line in $v-\ln p$ coordinate, M denoting lateral confinement (oedometer) modulus.

Similarly, in Modified Cam-clay, $\mathrm{d}\varepsilon_{\mathrm{a}}$, $\mathrm{d}\varepsilon_{\mathrm{v}}$ and $\mathrm{d}\varepsilon_{\mathrm{s}}$ are given in Eqs. 7-9, respectively. Note to apply $\mathrm{d}\varepsilon_{\mathrm{v}}$ and $\mathrm{d}\varepsilon_{\mathrm{s}}$ from Eqs. 8-9 to obtain $\mathrm{d}\varepsilon_{\mathrm{a}}$ in Eq. 7.

$$\mathrm{d}\varepsilon_{\mathrm{v}} = \frac{1}{1+e}\left[(\lambda-\kappa)\frac{2\left(\frac{q}{p}\right)d\left(\frac{q}{p}\right)}{M^2+\left(\frac{q}{p}\right)^2}+\lambda\frac{dp}{p}\right] \tag{8}$$

$$\mathrm{d}\varepsilon_{\mathrm{s}} = \frac{\lambda-\kappa}{1+e}\left[\frac{2\left(\frac{q}{p}\right)}{M^2-\left(\frac{q}{p}\right)^2}\right]\left[\frac{2\left(\frac{q}{p}\right)\mathrm{d}\left(\frac{q}{p}\right)}{M^2+\left(\frac{q}{p}\right)^2}+\frac{\mathrm{d}p}{p}\right] \tag{9}$$

Modeling Stress-Strain Observations

EPS-sand mixtures conforms less to the soil constitutive models than do most soils. This is because EPS-sand has one additional compressible inclusion (EPS beads), and the response of the mixture to be loaded is inherently more complex than the response of general soils, which complicates the constitutive law governing the behavior of the mixtures. The classical soil constitutive models may be weak in depicting the stress-strain behavior of EPS-sand mixtures. For example, as presented in Fig. 10, neither Cam-clay nor Modified Cam-clay was able to follow close enough the stress-strain responses of an EPS-sand specimen. The axial strain was either over-estimated under Cam-clay, or under-estimated under Modified Cam-clay.

Nevertheless, stress-strain observations indicate that the higher the EPS content η, the closer the observations approach Cam-clay modeling line; the lower the EPS content η, the closer the observations approach Modified Cam-clay modeling line. The stress-strain curves basically fluctuate between these two modeling lines depending on the EPS content. It was thus conceived to derive an improved model compromising Cam-clay and Modified Cam-clay to simulate the observations.

The volume of an EPS-sand unit was presumed to be divided into two parts, denoted by volumes $\zeta(\eta)$ and $(1-\zeta(\eta))$, respectively. Strain increments of volume $(1-\zeta(\eta))$ was depicted by using Cam-clay (i.e., Eqs. 5-7). Strain increments of volume $\zeta(\eta)$ was depicted by using Modified Cam-clay (i.e., Eqs. 7-9). The higher the EPS content η, the lower the $\zeta(\eta)$ value, which led to more volume of the unit modeled under Cam-clay and less volume modeled under Modified Cam-clay, and vice versa.

It was also presumed that the boundary conditions were constant in shear. Thus, the total strain increments ($\mathrm{d}\varepsilon_\mathrm{v}$, $\mathrm{d}\varepsilon_\mathrm{s}$, $\mathrm{d}\varepsilon_\mathrm{a}$) were equal to the sum of the strain increments of the two parts, i.e., ($\mathrm{d}\varepsilon_\mathrm{v}^A$, $\mathrm{d}\varepsilon_\mathrm{s}^A$, $\mathrm{d}\varepsilon_\mathrm{a}^A$) for volume $(1-\zeta(\eta))$, and ($\mathrm{d}\varepsilon_\mathrm{v}^B$, $\mathrm{d}\varepsilon_\mathrm{s}^B$, $\mathrm{d}\varepsilon_\mathrm{a}^B$) for volume $\zeta(\eta)$, as described in Eqs. 10-12, respectively.

$$\mathrm{d}\varepsilon_\mathrm{v} = (1-\zeta(\eta))\mathrm{d}\varepsilon_\mathrm{v}^A + \zeta(\eta)\mathrm{d}\varepsilon_\mathrm{v}^B \tag{10}$$

$$\mathrm{d}\varepsilon_\mathrm{s} = (1-\zeta(\eta))\mathrm{d}\varepsilon_\mathrm{s}^A + \zeta(\eta)\mathrm{d}\varepsilon_\mathrm{s}^B \tag{11}$$

$$\mathrm{d}\varepsilon_{\mathrm{a}} = (1-\zeta(\eta))\mathrm{d}\varepsilon_{\mathrm{a}}^{A} + \zeta(\eta)\mathrm{d}\varepsilon_{\mathrm{a}}^{B} \tag{12}$$

Merge Eqs. 5-7 and Eqs. 7-9, correspondingly, into Eqs. 10-12, the strain increment equations were expanded as follows.

$$\begin{aligned}\mathrm{d}\varepsilon_{\mathrm{v}} = {} & \left[1-\zeta(\eta)\right]\frac{1}{1+e}\left[\frac{\lambda-\kappa}{Mp}\left(\mathrm{d}q - \frac{q\mathrm{d}p}{p}\right) + \lambda\frac{\mathrm{d}p}{p}\right] + \\ & \zeta(\eta)\frac{1}{1+e}\left[(\lambda-\kappa)\frac{2\left(\frac{q}{p}\right)\mathrm{d}\left(\frac{q}{p}\right)}{M^{2}+\left(\frac{q}{p}\right)^{2}} + \lambda\frac{\mathrm{d}p}{p}\right]\end{aligned} \tag{13}$$

$$\begin{aligned}\mathrm{d}\varepsilon_{\mathrm{s}} = {} & \left[1-\zeta(\eta)\right]\frac{\lambda-\kappa}{(1+e)Mp}\left[\frac{\mathrm{d}q}{M-(q/p)} + \mathrm{d}p\right] + \\ & \zeta(\eta)\frac{\lambda-\kappa}{1+e}\left[\frac{2\left(\frac{q}{p}\right)}{M^{2}-\left(\frac{q}{p}\right)^{2}}\right]\left[\frac{2\left(\frac{q}{p}\right)\mathrm{d}\left(\frac{q}{p}\right)}{M^{2}+\left(\frac{q}{p}\right)^{2}} + \frac{\mathrm{d}p}{p}\right]\end{aligned} \tag{14}$$

$$
\begin{aligned}
\mathrm{d}\varepsilon_{\mathrm{a}} = \left[1-\zeta(\eta)\right]\Bigg\{ & \frac{\lambda-\kappa}{(1+e)Mp}\left[\frac{\mathrm{d}q}{M-(q/p)}+\mathrm{d}p\right]+ \\
& \frac{1}{3(1+e)}\left[\frac{\lambda-\kappa}{Mp}\left(\mathrm{d}q-\frac{q\mathrm{d}p}{p}\right)+\lambda\frac{\mathrm{d}p}{p}\right]\Bigg\}+ \\
\zeta(\eta)\Bigg\{ & \frac{\lambda-\kappa}{1+e}\left(\frac{2\left(\frac{q}{p}\right)}{M^2-\left(\frac{q}{p}\right)^2}\right)\left(\frac{2\left(\frac{q}{p}\right)\mathrm{d}\left(\frac{q}{p}\right)}{M^2+\left(\frac{q}{p}\right)^2}+\frac{\mathrm{d}p}{p}\right)+ \\
& \frac{1}{3(1+e)}\left[(\lambda-\kappa)\frac{2\left(\frac{q}{p}\right)\mathrm{d}\left(\frac{q}{p}\right)}{M^2+\left(\frac{q}{p}\right)^2}+\lambda\frac{\mathrm{d}p}{p}\right]\Bigg\}
\end{aligned}
\tag{15}
$$

There are four independent modeling parameters in the derived strain increment equations, i.e., M, κ, λ and $\zeta(\eta)$. Parameters M, κ and λ were obtained according to the conventions specified in Cam-clay. Parameter $\zeta(\eta)$ was obtained by simulating the stress-strain observations through least squares method. Based on the CD triaxial compression test results obtained in this investigation, the parameters for modeling the strain increments of EPS-sand mixtures are presented in Table 4. It is seen that over a half volume shall be modeled under Modified Cam-clay, and less than a half under Cam-clay, for the EPS-sand mixtures prepared within EPS content ranges of 0.5% to 2.5%.

The strain increment equations described in Eqs. 10-12 were proportion-dependent by introducing variant EPS content η. The strain increments were derived by compromising

Cam-clay and Modified Cam-clay, and were able to depict the complex stress-strain behavior of EPS-sand mixtures. Using the modeling parameters presented in Table 4, an improved modeling line was plotted in Fig. 10. The improved modeling line basically follows the observations, and is clearly superior to the modeling lines given by Cam-clay and Modified Cam-clay.

MODELING VERIFICATION

Modeling verification was implemented by plotting stress-strain increment equations (Eqs. 13-15) and test observations in a chart, as shown in Fig. 11 for EPS-sand mixtures at EPS content η=0.5% and Fig. 12 at η=1.5%. The solid lines represent the modeling curves, which broadly simulate the stress-strain observations, especially the deviatoric stress-axial strain observations, of specimens subjected to test conditions investigated in this study. Observations for EPS-sand mixtures prepared at η=0.5% were modeled better than for EPS-sand mixtures at η=1.5%. Marginal modeling deviations occurred to volumetric strain observations. Indeed, the deviations were either over-estimated or under-estimated, and no consistent deviation tendency was concluded. Notwithstanding, from the modeling simulations, the strain increment equations were derived favorably well to replicate stress-strain responses of EPS-sand mixtures, as least to model the CD shear behavior of specimens investigated in this study.

CONCLUSIONS

A laboratory testing program was carried out to evaluate the stress-strain characteristics and the shear strength of pure sand and EPS-sand specimens. Stress-strain increment equations were derived based on Cam-clay and Modified Cam-clay to model the stress-strain observations. Evaluation of the experimental results and modeling derivation obtained in this study led to the following conclusions:

(1) The CD triaxial test results of EPS-sand specimens showed an approximately hyperbolic stress-strain behavior and a fully contractive volumetric strain behavior. No clear peak strength was shown up throughout the axial strain as high as 15%. This response was significantly different from that of pure sand specimens, which showed a broadly defined peak shear strength and dilatant behavior for the relative density used in this study.

(2) The influence of EPS content on the stress-strain behavior of EPS-sand specimens was significant. Specifically, EPS-sand specimens prepared at relatively high EPS content (η=1.5% and 2.5%) exhibited: a) substantial contraction during consolidation, b) a piecewise (two-segment) linear K_f line, and c) a non-negligible cohesion intercept. Pure sand and EPS-sand specimens of low EPS content (η=0.5%) had straight K_f lines intercepting the origin.

(3) The shear strength of EPS-sand mixtures was affected by the EPS content. The shear strength decreased with increasing EPS content. An EPS content in the order of 0.5% was suggested for producing EPS-sand mixtures, which yielded a reasonable combination of the unit weight and shear strength of the mixture, at least in the investigation of this study. Accordingly, infrastructure works subjected to comparatively low confining pressures (e.g. utilities trench backfills) can particularly benefit from the addition of EPS beads.

(4) Strain increment equations were derived by compromising Cam-clay and Modified Cam-clay. The equations were proportion dependent by introducing the variant EPS content η. The other four model parameters can be calibrated from CD triaxial test results. Equations were verified as reasonably acceptable laws governing the strength and deformation characteristics of EPS-sand mixtures prepared at varying EPS contents, at least those investigated in this study.

ACKNOWLEDGEMENTS

Contents described in this study were extended from the conference paper included in the ASCE GSP 192, GeoHunan International Conference: Challenges and Recent Advances in Pavement Technologies and Transportation Geotechnics. The selection and recommendation of this study by the Conference Organizing Committee is appreciated. The work was supported by a grant of National Natural Science Foundation of China (50708031).

References

Aytekin, M. (1997). Numerical modeling of EPS geofoam used with swelling soil. Geotextiles and Geomembranes, 15(1-3), 133-146.

Bowles, J. E. (1992). Engineering Properties of Soils and their Measurement, 4th Edition. McGraw Hill, Inc., New York.

Chun, B. S., Lim, H. S., Sagong, M., Kim, K. (2004). Development of a hyperbolic constitutive model for expanded polystyrene (EPS) geofoam under triaxial compression tests. Geotextiles and Geomembranes, 22(4), 223-237.

Desai C. and Siriwardane H. J. (1984). Constitutive Laws for Engineering Materials with Emphasis on Geologic Materials. Prentice Hall, New Jersey.

Duskov, M. (1997). Measurements on a flexible pavement structure with an EPS geofoam sub-base. Geotextiles and Geomembranes, 15(1-3), 5-27.

Fang, P. F., Zhu, X. R., and Li, Y. F. (2006). Experiment study on static and dynamic behavior of EPS. Ground Modification and Seismic Mitigation, GSP 152, ASCE, Reston, Va., 223-230.

Greeley, T. R. (1997). Review of expanded polystyrene (EPS) properties, performance and new applications. ASTM STP 1320, West Conshohocken, Pa., 226-239.

Hazarika, H. and Okuzono, S. (2004). Modeling the behavior of a hybrid interactive system involving soil, structure and EPS geofoam. Soils and Foundations, 44(5), 149-162.

Hazarika, H. (2006). Stress-strain modeling of EPS geofoam for large-strain applications. Geotextiles and Geomembranes, 24(2), 79-90.

Head, K. H. (1982). Manual of Soil Laboratory Testing. Vol. 2. Pentech Press Ltd., London.

Horvath, J. S. (1994). Expanded polystyrene (EPS) geofoam: An introduction to material behavior. Geotextiles and Geomembranes, 13(4), 263-280.

Horvath, J. S. (1997). The compressible inclusion function of EPS geofoams. Geotextiles and Geomembranes, 15(1-3), 77-120.

Horvath, J. S. (2004). Geofoam compressible inclusions: The new frontier in earth retaining structures. Geotechnical Engineering for Transportation Projects, GSP 126 II, ASCE, Reston, Va., 1925-1934.

Horvath, J. S. (2008). Using EPS-block geofoam for levee rehabilitation and construction. Geosustainability and Geohazard Mitigation, GSP 178, ASCE, Reston, Va., 765-772.

Ikizler, S. B., Aytekin, M., and Nas, E. (2008). Laboratory study of expanded polystyrene (EPS) geofoam used with expansive soils. Geotextiles and Geomembranes, 26(2), 189-195.

Indraratna, B., Wijewardena, L. S. S., and Balasubramaniam, A. S. (1993). Large-scale triaxial testing of greywacke rockfill. Geotechnique, 43(1), 37–51.

Liu, H. L., Deng, A., Chu, J. (2006). Effect of different mixing ratios of polystyrene pre-puff beads and cement on the mechanical behaviour of lightweight fill. Geotextiles and Geomembranes, 24(6), 339-348.

Marachi, N. D., Chan, C. K., and Seed, H. B. (1972). Evaluation of properties of rockfill materials. Journal of the Soil Mechanics and Foundation Division, 98(SM1), 95-114.

Ortigao, J. A. R. (1995). Soil Mechanics in the Light of Critical State Theories An Introduction. A.A. Balkema, Brookfield.

Riad, H. L. and Horvath, J. S. (2004). Analysis and design of EPS-geofoam embankments for seismic loading. Geotechnical Engineering for Transportation Projects, GSP 126 II, ASCE, Reston, Va., 2028-2037.

Schofield A. N. and Wroth C. P. (1968). Critical State Soil Mechanics. McGraw-Hill, London.

Snow, C. L. and Nickerson, C. R. (2004). Case study of EPS Geofoam lightweight fill for settlement control at bridge approach embankment. Geotechnical Engineering for Transportation Projects, GSP 126 I, ASCE, Reston, Va., 580-589.

Wang, Z. L., Li, Y. C., and Wang, J.G. (2006). Numerical analysis of attenuation effect of EPS geofoam on stress-waves in civil defense engineering. Geotextiles and Geomembranes, 24(5), 265-273.

Wen, Z., Sheng, Y., Ma, W. and Qi, J. L. (2008). In situ experimental study on thermal protection effects of the insulation method on warm permafrost. Cold Regions Science and Technology, 53(3), 369-381.

Wong, H., Leo, C. J. (2006). A simple elastoplastic hardening constitutive model for EPS geofoam. Geotextiles and Geomembranes, 24(5), 299-310.

Zarnani, S. and Bathurst, R. J. (2009). Influence of constitutive model on numerical simulation of EPS seismic buffer shaking table tests. Geotextiles and Geomembranes, 27(4), 308-312.

Zornberg, J. G., Cabral, A. R. and Viratjandr, C. (2004). Behaviour of tire shred – sand mixtures. Canadian Geotechnical Journal, 41(2), 227-241.

Zhu, W., Li, M. D., Zhang, C. L. and Zhao, G. (2008). Density and strength properties of sand-expanded polystyrene beads mixture. Characterization, Monitoring, and Modeling of GeoSystems, GSP 179, ASCE, Reston, Va., 36-43.

List of Table Captions

Table 1: Index property of tested materials.

Material	Specific gravity	Bulk unit weight (kN/m^3)	Effective size D_{10} (mm)	Classification USCS	Classification AASHTO
Sand	2.62	15.4 (min.), 18.9 (max.)	0.1	SW	A-3 (0)
EPS bead	0.03	0.15	2.2	-	-

Table 2: Summary of testing program.

Series	EPS content η (by weight, %)	EPS volume ratio ς (%)	Bulk unit weight (kN/m^3)	Consolidation pressure (kPa)
1	0	0	17.0	100, 200, 300 and 400
2	0.5	30	12.6	100, 200, 300 and 400
3	1.5	57	8.2	100, 200, 300 and 400
4	2.5	69	6.3	100, 200, 300 and 400

Table 3: Strength parameters of K_f lines and Mohr Coulomb envelopes.

EPS content	K_f line			Mohr Coulomb envelope	
η (%)	α (°)	a (kPa)	R^2	ϕ_{cd} (°)	c (kPa)
0	31.4	0.0	0.99	37.6	0.0
0.5	21.3	0.0	0.99	23.0	0.0
1.5 *	9.1	40.0	0.99	9.4	41.0
1.5 **	18.3	0.0	0.84	19.3	0.0
2.5 *	10.8	16.4	0.95	11.0	16.7
2.5 **	15.7	0.0	0.87	16.3	0.0

*: the lower segment of K_f line; **: the upper segment of K_f line.

Table 4: Modeling parameters.

η (%)	M	κ	λ	$\zeta(\eta)$
0.5	1.47	0.035	0.087	0.81
1.5	1.11	0.092	0.239	0.65
2.5	0.91	0.140	0.400	0.52

List of Figure Captions

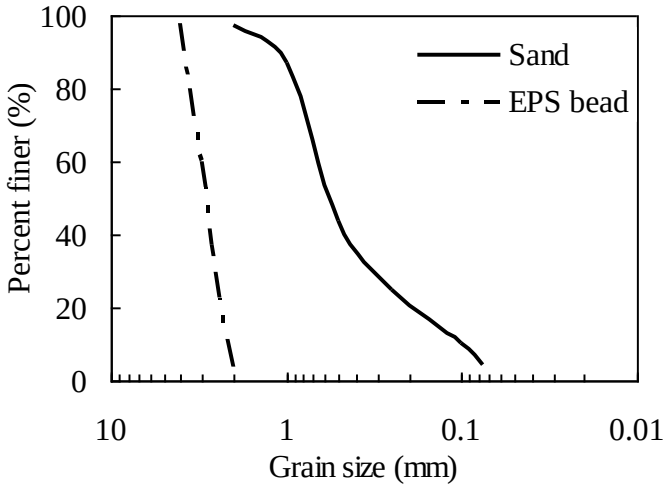

Fig. 1: Gradation curves of sands and EPS beads.

Fig. 2: EPS-sand mixture.

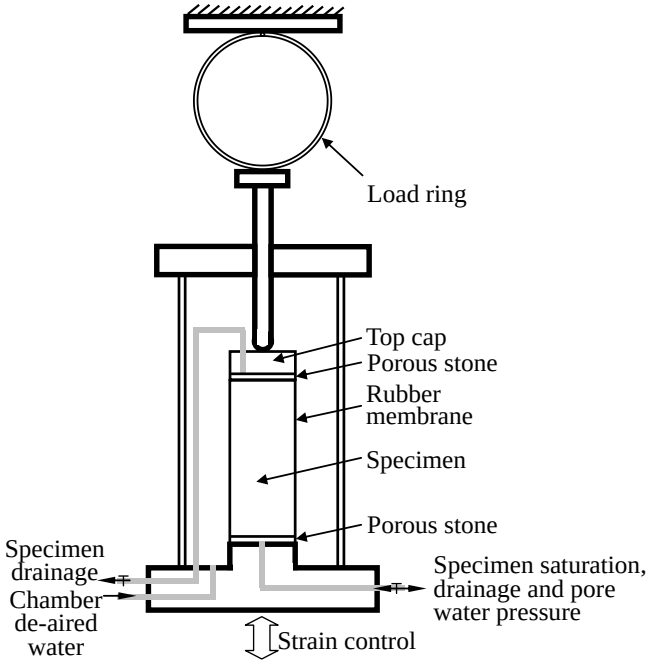

Fig. 3: Schematic diagram of the triaxial cell.

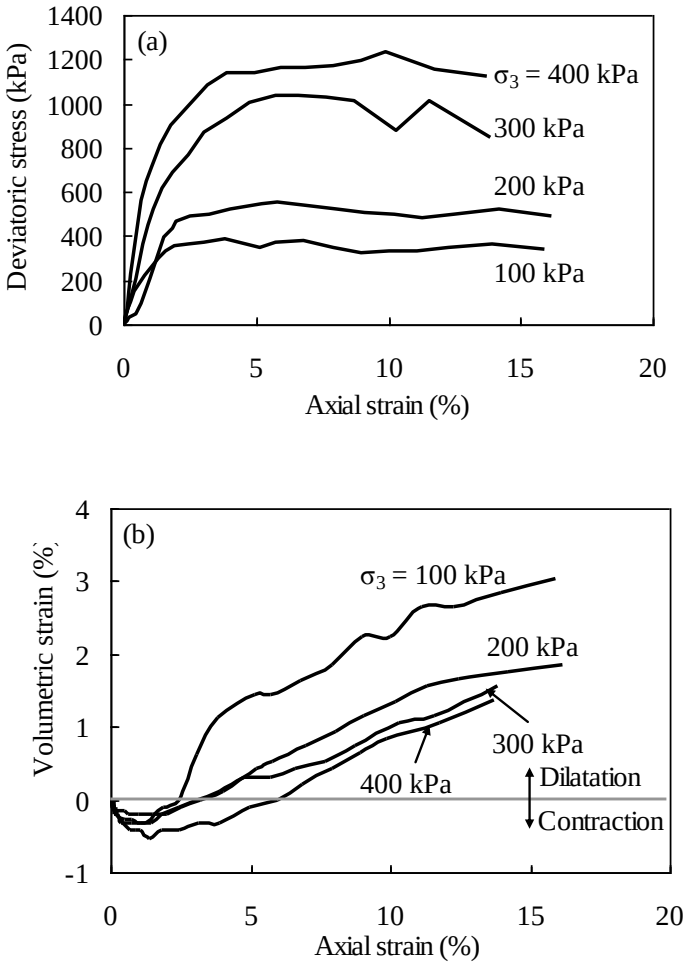

Fig. 4: Results of tests on pure sand (series 1): (a) deviatoric stress-strain behavior; (b) volumetric strain behavior.

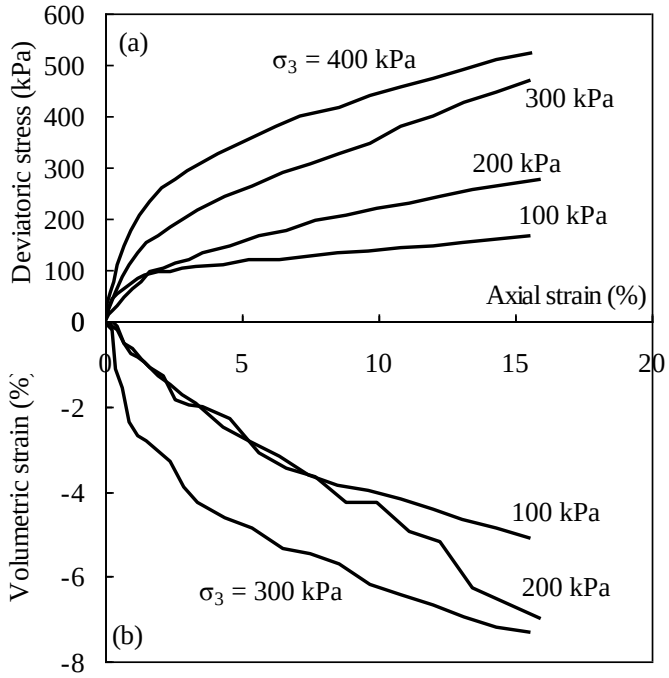

Fig. 5: Results of tests on EPS-sand at η=0.5% (series 2): (a) deviatoric stress-strain behavior; (b) volumetric strain behavior.

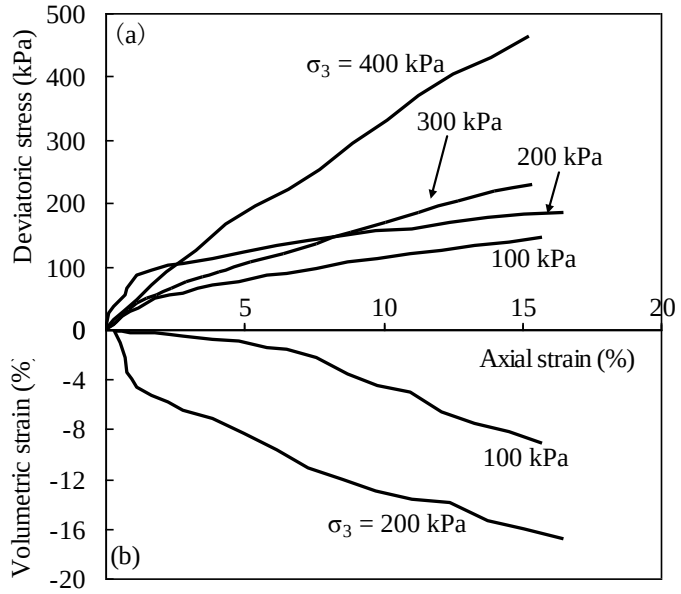

Fig. 6: Results of tests on EPS-sand at η=1.5% (series 3): (a) deviatoric stress-strain behavior; (b) volumetric strain behavior.

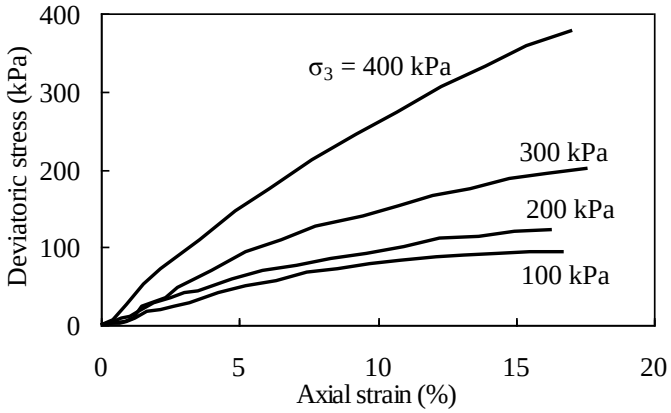

Fig. 7: Results of tests on EPS-sand at η=2.5% (series 4): deviatoric stress-strain behavior.

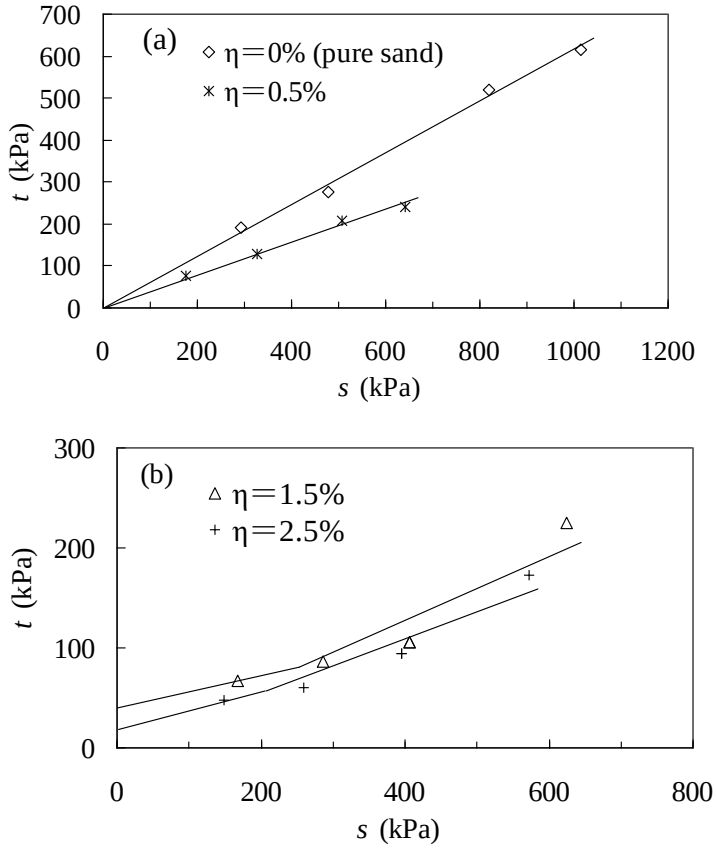

Fig. 8: K_f lines of specimens at different EPS contents: (a) η=0% (pure sand) and 0.5%; (b) η=1.5% and 2.5%.

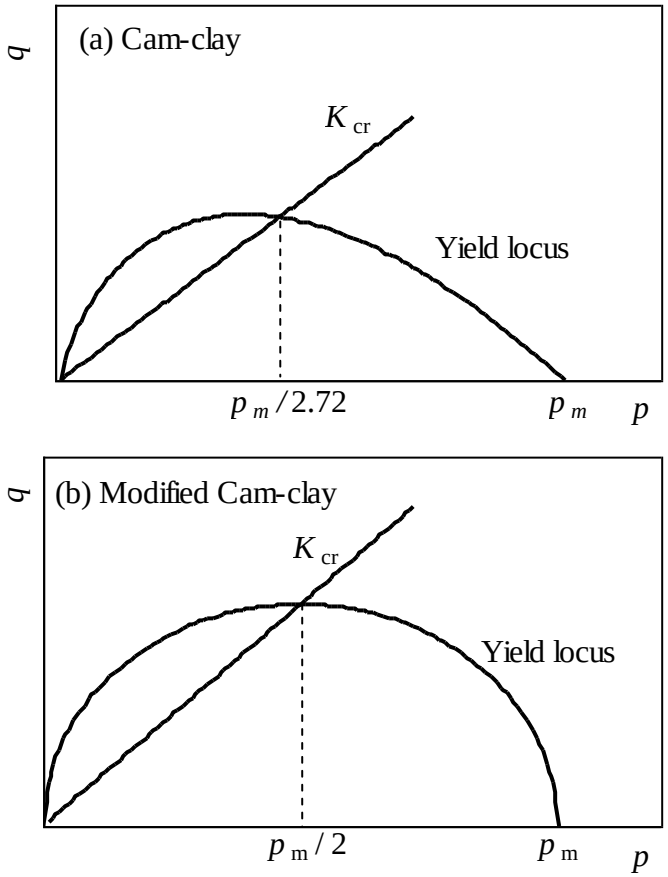

Fig. 9: Different assumptions for yield loci: (a) Cam-clay; (b) Modified Cam-clay.

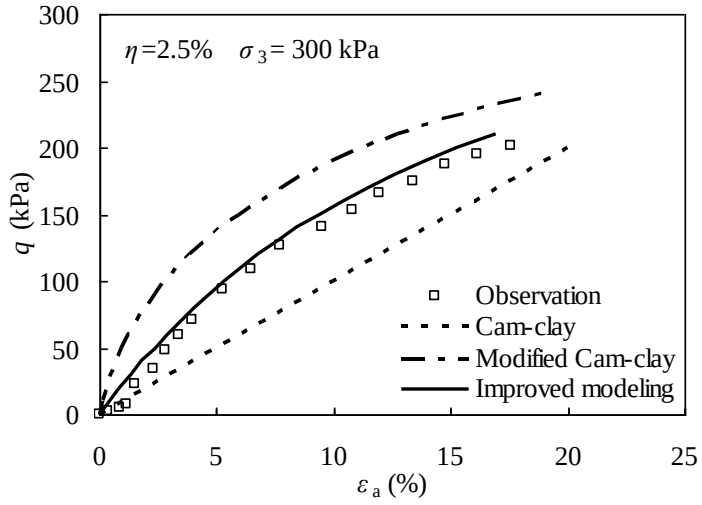

Fig. 10: Deviatoric stress-axial strain simulations.

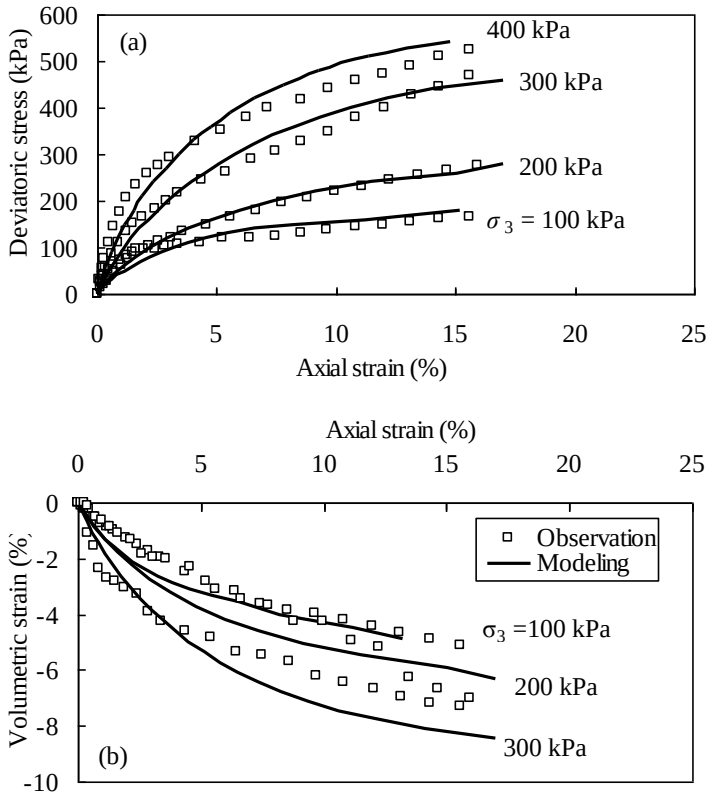

Fig. 11: Modeling stress-strain observations for EPS-sand mixture at EPS content η=0.5%: (a) deviatoric stress-axial strain relation; (b) volumetric strain-axial strain relation.

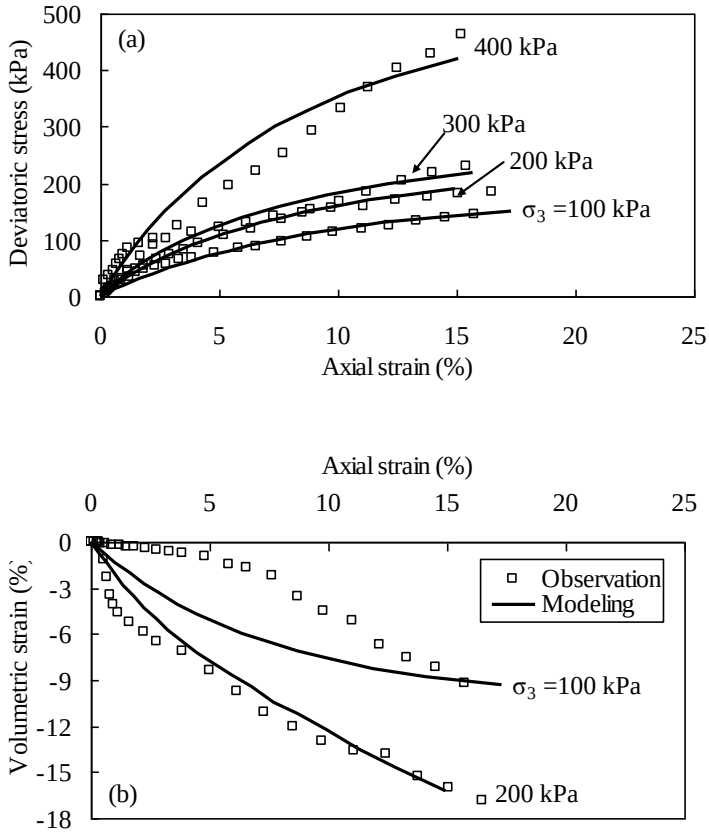

Fig. 12: Modeling stress-strain observations for EPS-sand mixture at EPS content η=1.5%: (a) deviatoric stress-axial strain relation; (b) volumetric strain-axial strain relation.